$4^{th}$ URSI AT-RASC, Gran Canaria, 19 – 24 May 2024

# Topologically Protected Electromagnetic Waveguiding in All-Dielectric Meta-Waveguides

Menglin L. N. Chen* and Rui Zhou
Department of Electrical and Electronic Engineering, The Hong Kong Polytechnic University, Hong Kong, China

## Abstract

Waveguiding devices are fundamental components in communication systems. While operation frequencies of communication bands are migrating to millimeter wave regime, design requirements for electronic components become more demanding. With the rapid development of topological photonics, it has been found that topology of artificial structures can provide prospects for optical circuits to achieve unprecedented features. Inspired by the idea of topology, here, we propose a new protection mechanism for dielectric waveguides to achieve robust electromagnetic wave propagation against path bends or defects. By decorating the boundaries of the conventional waveguide with valley photonic crystals, topologically protected hybrid modes consisting of transverse electric modes and valley edge states are generated. The proposed meta-waveguide is highly compatible with substrate-integrated waveguide technology. By leveraging the idea of topology to waveguiding devices, we introduce the topological protection into conventional waveguiding modes, which would largely improve the performance of communication systems.

## 1 Introduction

The next-generation communication system exploits higher frequencies. From new materials to novel design methods, microwave and millimeter wave technologies are embracing great opportunities as well as challenges. Waveguides have been widely used in communication systems due to their incomparable performances and compact sizes. However, the degradation of signals will inevitably appear at defects or intersections when there is a mode mismatching [1]. With the development of topological photonics, robust waveguiding at the interface of two artificial materials with different topologies could be achieved [2]. This discovery provides opportunities for the realization of robust waveguide design [3, 4]. In topological photonics, spin-Hall and valley-Hall photonic crystals (PhCs) have been exploited to support topologically protected electromagnetic (EM) transmission [5, 6]. The proposed topological spin and valley waveguides are prominent for integrated circuits, from on-chip communication to channel intersection and routing [7, 8]. However, the topological edge states are usually tightly confined at the interface, which not only limits the power capacity but also makes them incompatible with the modes supported in conventional circuits.

To address the above issues, we devise a topological meta-waveguide which is composed of an air channel sandwiched between two valley PhCs with opposite valley-Chern numbers. The EM modes within two band gaps are observed. Valley-locked edge states appear at the two PhC-air interfaces in both frequency bands. Interestingly, waveguide modes also exist in the air region in the higher frequency band. This fact is jointly determined by the bulk-edge correspondence and the position of the light line. The presence of valley-locked edge states contributes to the robust transmission of the waveguide modes in the air channel. Effective coupling from the hybrid modes in the meta-waveguide to the modes in substrate integrated waveguide (SIW) is achieved. Our design combines the advantages of integrated waveguides and topological PhCs, providing a novel approach to integrating the topological effects into conventional circuits.

## 2 Theory and Model

### 2.1 Bulk state analysis

A PhC arranged in a triangular lattice is shown in Fig. 1(a). The black rhombus and hexagon show the original unit consisting of two types of dielectric rods, A and B. Their diameters are denoted by $d_\mathrm{A}$ and $d_\mathrm{B}$, respectively. The finite element method is used to simulate the PhC. As shown in Fig. 1(b), when $\Delta d = 0\left(\Delta d = d_\mathrm{A} - d_\mathrm{B}, d_{\mathrm{A/B}} = 0.48a_0\right)$, band degeneracy occurs at the $K/K'$ points at two frequencies (black dashed lines). When the inversion symmetry of the unit cell is broken by setting $\Delta d \neq 0$, two complete band gaps will appear (black solid lines). When $\Delta d = \pm 0.16a_0$, there are two band gaps at 13.5-15.5 GHz ($f_1$) and 28-32 GHz ($f_2$). We use the Berry curvature to verify the topological state of the PhCs. The Berry connection of the four bands (bands 1,2,4,5) can be defined as:

$$\vec{A}(\vec{k}) \equiv i\left\langle u_{\vec{k}}\left|\nabla_{\vec{k}}\right|u_{\vec{k}}\right\rangle = i\oint_{unitcell} \mathrm{d}^2 r \varepsilon(\vec{r}) u_{\vec{k}}^* \left[\nabla_{\vec{k}} u_{\vec{k}}\right], \quad (1)$$

where $u_{\vec{k}}$ is the electromagnetic fields. Note that eigenstate amplitude is normalized such that $\langle u_{\vec{k}} \mid u_{\vec{k}}\rangle = 1$. The Berry

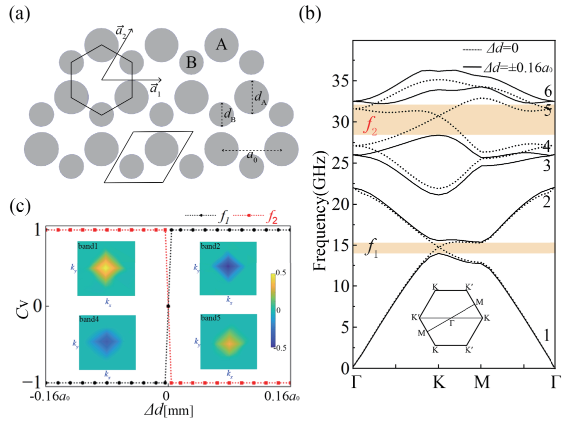


**Figure 1.** The proposed valley PhC. (a) Geometry of the PhC. (b) Band structures of PhCs. (c) The calculated Valley-Chen number as a function of $\Delta d$.

curvature $\Omega(\vec{k})$ is obtained by:

$$\Omega(\vec{k}) \equiv \nabla_{\vec{k}} \times \vec{A}(\vec{k}) = \frac{\partial A_y(\vec{k})}{\partial k_x} - \frac{\partial A_x(\vec{k})}{\partial k_y}. \qquad (2)$$

As a result, the valley-Chern number $C_V = 1$ for bands 1 and 5, and $C_V = -1$ for bands 2 and 4 [Fig. 1(c)]. The change in the valley-Chern number directly proves that the system undergoes a topological phase transition as $\Delta d$ changes, which is a necessary condition for the emergence of topological edge states.

## 2.2 Waveguiding state analysis

Different from the existing methods by building the interfaces between two structures with different topologies, here, we construct an air channel (can be considered to have a $C_V = 0$) with the width of $g_0$ sandwiched between two valley PhCs with opposite valley-Chern numbers, as shown in Fig. 2(a). As shown in the dispersion diagrams of Figs. 2(b) and (c), for fixed $g_0$, one band appears in each band gap. The essential difference of these states within the two band gaps is that the states near the $K/K'$ valley are below air line (as indicated by the black lines) in $f_1$ but are above the air line in $f_2$. Consequently, in $f_1$ band gap, the states become surface edge states concentrated at the PhC-air domain walls. As can be seen from the plotted electric-field distributions and the Poynting vectors, when $g_0 = 2l$, within $f_1$, the states below the light line are analogue to the surface states that are confined tightly in the dielectric region [9]. Effective energy flow only exists at the domain walls and no mode is propagating in the air channel. In $f_2$ band gap, all states exist above the light line [Fig. 2(c)], indicating that there is a leakage of mode into the air region. When $g_0 = 2l$, the electric fields and Poynting vectors clearly show that a wave-guiding mode is generated in the core air channel and couples with the valley-locked edge states, forming a hybrid mode.

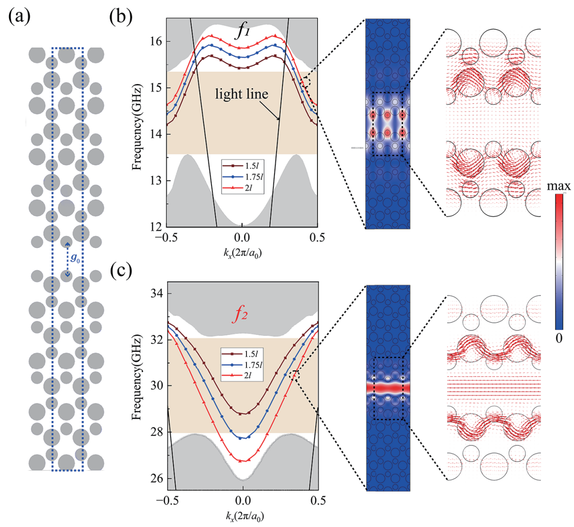


**Figure 2.** The proposed topological interface. (a) Geometry of the supercell (enclosed by blue dotted line). The band structures, electric fields and Poynting vectors of waveguiding states for different $g_0$ in (b) lower frequency band, $f_1$ and (c) higher frequency band $f_2$.

# 3 Topological Meta-Waveguide Design

## 3.1 Interconnection with substrate integrated waveguides

The proposed meta-waveguide has an air channel with adjustable width, providing an additional degree of freedom for manipulating its eigenstates. Therefore, the intersection between the meta-waveguide and existing circuit components are much easier to achieve. Considering the similarity of the wave-guiding mode supported at the central air region of the meta-waveguide with the conventional transverse electric mode, we connect the meta-waveguide with standard SIWs which support $TE_{10}$ mode. The coupling of the modes in different frequency bands is shown in Fig. 3.

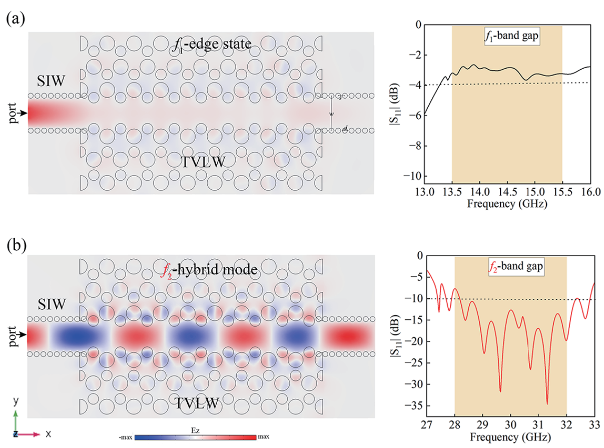


**Figure 3.** The meta-waveguide interconnected with standard SIWs. The electric fields and $S_{11}$ in (a) lower frequency band, $f_1$ and (b) higher frequency band $f_2$.

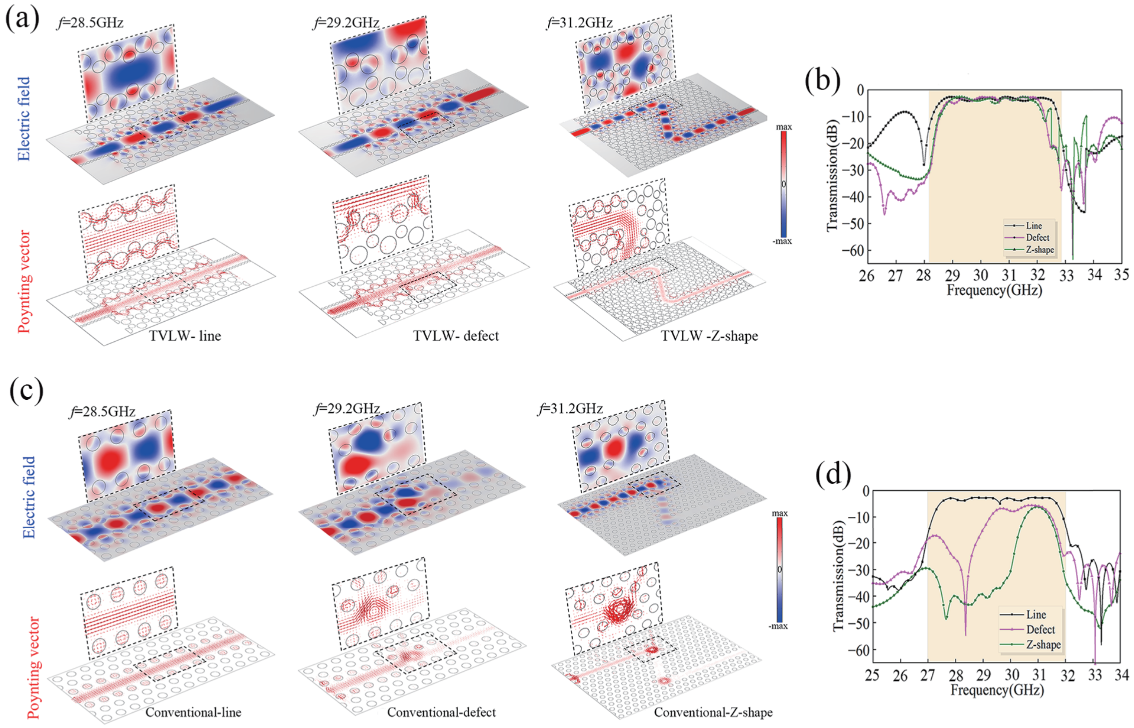


**Figure 4.** Robustness analysis of the proposed meta-waveguide compared with a conventional photonic crystal waveguide. (a) Electric fields, Poynting vectors and (b) transmission rates of three topological waveguides in the $f_2$ frequency band. (c) Electric fields, Poynting vectors and (d) transmission rates of three conventional waveguides.

Clearly, when there is no supported mode in the air region, the meta-waveguide and SIW encounter severe mode mismatching with reflection coefficients higher than $-4$ dB [Fig. 3(a)]. On the contrary, a good matching with reflection coefficients lower than $-10$ dB is achieved within the whole operation frequency band of $f_2$ [Fig. 3(b)]. These results imply that the modes being supported in the air channel ensure an effective mode conversion from conventional waveguides to the meta-waveguide.

### 3.2 Robustness analysis and comparison

The robustness of the proposed meta-waveguide is verified through full-wave simulations. When $g_0 = 2l$, three types of waveguides are demonstrated. Fig. 4(a) shows the electric-field distributions and Poynting vectors of the straight, defective, and Z-shaped meta-waveguide at different frequencies. Obviously, the hybrid wave-guiding modes supported in the meta-waveguide present the features of topological protection with robust EM transmission against defects and bends. In the defective waveguide, the valley-locked edge states can bypass the defect (black dotted rectangle) and the hybrid mode is reconstructed without backscattering. Meanwhile, when the EM waves propagate along the Z-shaped bend, there is no loss and the hybrid mode can smoothly bypass the 60-degree bend. The simulated transmission coefficients of the three waveguides are shown in Fig. 4(b). The transmission loss is less than $-3$ dB within the whole operation frequency band. For comparison, a conventional PhC waveguide with the same material parameters and size is designed and simulated. It is found that when the conventional waveguide encounters defects and bends, strong scattering and local resonance will occur, and its transmission loss far exceeds 10 dB, as shown in Figs. 4(c) and (d). Therefore, it is confirmed that the wave-guiding mode supported in the designed meta-waveguide presents the feature of topological protection as in valley PhCs although a conventional transverse electric mode is in presence in the air channel.

## 4 Conclusion

In summary, a novel all-dielectric meta-waveguide by decorating the surfaces of a conventional hollow waveguide with valley PhCs has been proposed. By enabling the coupling of air modes and topological edge states, a hybrid mode consisting of a transverse electric mode and valley-locked edge states has been generated. Most importantly, the feature of topological protection of the hybrid modes has been demonstrated in millimeter wave regime. Benefiting from the unique mode feature, an efficient intersection between the proposed meta-waveguide and a standard SIW has been achieved. Our wave-guiding mechanism can be used in more general cases such as feeding/matching network design, high-capacity energy transport, and high-quality signal transmission in millimeter wave integrated circuits.

## 5 Acknowledgements

This work was financially supported by the National Natural Science Foundation of China (62301470) and the Hong Kong Polytechnic University Start-up fund for RAPs (No. BD2P).

## References

[1] Z. Xu, X. Yin, and D. F. Sievenpiper, "Adiabatic Mode-Matching Techniques for Coupling Between Conventional Microwave Transmission Lines and One-Dimensional Impedance-Interface Waveguides," *Phys. Rev. Appl.*, **11**, 4, April 2019, pp. 004071.

[2] R. Zhou, H. Lin, H. Y. Liu, X. T. Shi, R. X. Tang, Y. J. Wu, and Z. H. Yu, "Topological Edge States of Kekulé-Type Photonic Crystals Induced by a Synchronized Rotation of Unit Cells," *Phys. Rev. A*, **104**, 3, September 2021, pp. L031502.

[3] Z. Lan, M. L. N. Chen, F. Gao, S. Zhang, and W. E. I. Sha, "A Brief Review of Topological Photonics in One, Two, and Three Dimensions," *Reviews in Physics*, **9**, August 2022, pp. 100076,

[4] S. J. Li, M. L. N. Chen, Z. Lan, and P. Li, "Coexistence of Large-Area Topological Pseudospin and Valley States in a Triband Heterostructure System," *Opt. Lett.*, **48**, 17, September 2023, pp. 1–5.

[5] J. Zhang, X. Zhang, and A. A. Kishk, "Study of Bend Discontinuities in Substrate Integrated Gap Waveguide," *IEEE Microw. Wirel. Compon. Lett.*, **27**, 3, March. 2017, pp. 221–223.

[6] D. Bisharat, R. Davis, Y. Zhou, P. Bandaru, and D. Sievenpiper, "Photonic Topological Insulators: A Beginner's Introduction [Electromagnetic perspectives]," *IEEE Trans. Antennas Propag.*, **63**, 3, June 2021, pp. 112–124.

[7] M. L. N. Chen, L. J. Jiang, Z. Lan, and W. E. I. Sha, "Pseudospin-Polarized Topological Line Defects in Dielectric Photonic Crystals," *IEEE Trans. Antennas Propag.*, **68**, 1, January 2020, pp. 609–613.

[8] J. W. Dong, X. D. Chen, H. Zhu, Y. Wang, and X. Zhang, "Valley Photonic Crystals for Control of Spin and Ttopology," *Nat. Mater.*, **16**, 3, March 2017, pp. 298-302.

[9] M. L. N. Chen, L. J. Jiang, Z. Lan, and W. E. I. Sha, "Local orbital-angular-momentum dependent surface states with topological protection," *Opt. Experss*, **28**, 10, May 2020, pp. 14428–14435.